Journal of the European Ceramic Society 20 (2000) 1929–1938

SiC/SiC minicomposites with structure-graded BN interphases

S. Jacques *, A. Lopez-Marure, C. Vincent, H. Vincent, J. Bouix

Laboratoire des Multimatériaux et Interfaces — UMR 5615 CNRS/University of Lyon 1, 43, boulevard du 11 Novembre 1918, F–69622 Villeurbanne Cedex, France

Received 28 October 1999; received in revised form 10 February 2000; accepted 14 February 2000

Abstract

BN interphases in SiC/SiC minicomposites were produced by infiltration of fibre tows from BF_3–NH_3–H_2 gaseous system. During interphase one-step processing, the tow travels through a reactor containing a succession of different hot areas. By TEM characterization, the BN interphases were found to be made of a structural gradient: from isotropic to highly anisotropic. The very first coating is poorly organised and allows to protect the fibre from a further chemical attack by the reactant mixture. The minicomposites were tensile tested at room temperature with unloading-reloading cycles. The BN interphases act as mechanical fuses; the fibre/matrix bonding intensity ranges from weak to rather strong depending on the tow travelling rate during interphase infiltration. The specimen lifetimes at 700°C under a constant tensile loading were measured in dry and moist air. Compared to a pyrocarbon reference interphase, the BN interphases significantly improve the oxidation resistance of the SiC/SiC minicomposites.

Keywords: BN; Composites; Electron microscopy; Interphase; Oxidation resistance; SiC/SiC

1. Introduction

In SiC/SiC type ceramic matrix composites, a good toughness can be achieved by adding between the fibre and the brittle matrix a thin film of a compliant material called "interphase".[1] If highly anisotropic pyrolytic (ex-BF_3) boron nitride can replace advantageously the poor oxidation resistance pyrocarbon (PyC), its chemical vapour infiltration (CVI) processing requires to protect the fibre from a chemical attack with an isotropic BN pre-coating obtained with less aggressive conditions.[2,3] Thus, in the case of a classical static isothermal CVI, the BN interphase must be infiltrated by following several separate steps (i.e. changing the boron precursor gas and CVI parameters during the experiment...).

The aim of the present work was to prepare within 1D minicomposites BN interphases with structural gradients by using a one-step continuous dynamic CVI process and to characterize these minicomposites.

2. Experimental procedure

2.1. Samples

The samples used in this study were SiC/SiC minicomposites. A minicomposite is a 1D model composite. It consists of a tow in which the BN or PyC interphase and then the SiC matrix are infiltrated by CVI. The tow is composed of around 500 Hi-Nicalon fibres (monofilaments) (from Nippon Carbon, Japan) (Fig. 1).

The geometry of the minicomposite is simpler than that of the actual composite. It can properly simulate its behaviour and specially enables to determine the interphase properties.

In our case, the fibre volume fraction V_f of the minicomposites was about 20% (measured by weighing).

2.2. Interphase processing

The process used for the interphase preparation was a new process called thermal gradient-chemical vapour infiltration (TG-CVI).[4,5] The reactor was a hot wall furnace: a graphite susceptor (length: 35 cm) placed inside a silica tube (inner diameter: 24 mm) is heated by induction. The fibre tow was unwound from a first spool

* Corresponding author.
E-mail address: sylvain.jacques@adm.univ-lyon1.fr (S. Jacques).

0955-2219/00/$ - see front matter
PII: S0955-2219(00)00064-9

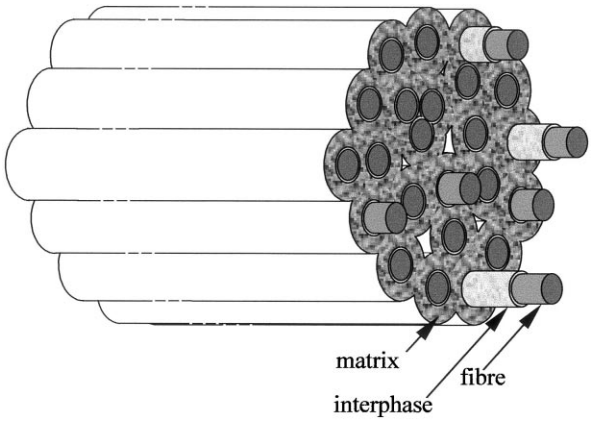

Fig. 1. Schematics of a minicomposite prepared by CVI (for clarity, only a few fibres out of the 500 that constitute a whole tow are represented).

through the susceptor. The outlet reactor winding around a second spool controlled the fibre travelling rate r.

For BN interphase processing, a specific temperature profile was obtained inside the susceptor thanks to a variable pitch of induction heating coil turns (Fig. 2). Thus, the reactor contained three distinct hot areas with respectively a "low" temperature ($<1100°C$), a medium maximum temperature ($\sim 1150°C$) and a high one ($\sim 1250°C$). The control of the fibre displacement (r) through the hot areas allowed to determine the duration of the CVI treatment and consequently the interphase thickness. BF_3/NH_3 were the gas precursors of BN, argon was used as the gas vector but also to dilute the reactive species. The total gas flow rate Q was 60 cm^3 min^{-1}. The gas composition was: $Q_{NH_3}/Q_{BF_3}=0.5$ and $Q_{Ar}/(Q_{BF_3}+Q_{NH_3})=0.222$. The gas pressure was 20 kPa.

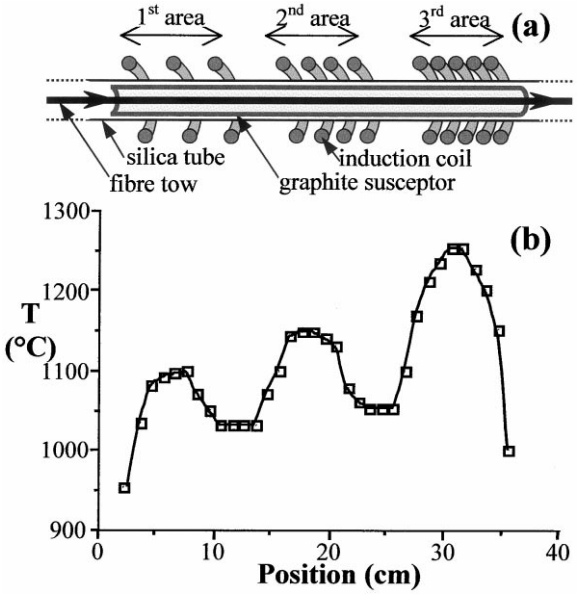

Fig. 2. Schematics of the TG-CVI reactor (a) and susceptor temperature profile (b).

Three batches of minicomposites called 1, 2 and 3 containing BN interphases obtained respectively with a tow rate r of 2, 2.5 and 3 m/h were prepared.

A fourth batch called 0 with a pyrocarbon (PyC) interphase was also prepared in order to be used as a reference. The pyrocarbon was infiltrated by CVI but using a classical induction device (i.e. constant pitch of coil turns and consequently one hot area) from propane ($Q_{C_3H_8}=9.6$ cm^3 min^{-1}) under a pressure of 10 kPa and with $r=6$ m/h. Argon was used as the gas vector ($Q_{Ar}=38.5$ cm^3 min^{-1}). The maximum temperature in the centre of the hot area was 1050°C. Unlike the BN infiltration, gas inlet and outlet were permuted in order to have a gas flux and a tow displacement in reverse direction and thus a good adhesion between the fibre and the coating.[6]

2.3. SiC matrix processing

The SiC matrix was infiltrated by classical CVI in a second reactor from CH_3SiCl_3/H_2 precursor gases at 1100°C. The ratio $Q_{H_2}/Q_{CH_3SiCl_3}$ was 0.75, the total gas flow rate was 70 cm^3 min^{-1} and pressure 5 kPa. The duration of matrix infiltration was 5 h.

2.4. Charaterization

2.4.1. Mechanical behaviour

The minicomposites were tensile tested at room temperature with unloading-reloading cycles using a MTS-Adamel DY-22 machine (Ivry sur Seine, France) equipped with a 1 kN load cell. The minicomposite ends were glued within 50 mm distant metallic tubes that were then gripped into the testing machine jaws. The crosshead speed was 0.1 mm/min. The strain was measured with an extensometer (Ingström, Cat. No. 2620-602, travel: 2.5 mm, type dynamic, code value 136) directly gripped on the minicomposite itself. The extensometer gauge length (L_g) was 40 mm. Five tests per batch were carried out.

In order to evaluate the fibre/matrix bonding, the interfacial shear stress τ was estimated by following the same methods as those used by Bertrand et al.[7] They are presented in outline below.

The first method considers, for unloading-reloading cycles, the width $\delta\Delta$ of the hysteresis loop at a given stress σ'. τ is given by Eq. (1):[8]

$$\tau=\frac{b_2N(1-a_1V_f)^2R_f}{2V_f^2E_m}\frac{\sigma_p^2}{\delta\Delta}\frac{\sigma'}{\sigma_p}\left(1-\frac{\sigma'}{\sigma_p}\right) \quad (1)$$

with

$$a_1=\frac{E_f}{E_0}$$

and

$$b_2 = \frac{(1+\nu)E_m[E_f + (1-2\nu)E_0]}{E_f[(1+\nu)E_f + (1-\nu)E_0]}$$

where σ_p is the maximum stress of the cycle, E_0 is the initial Young's modulus of the minicomposite, E_f (~280 GPa) and E_m (~400 GPa) are the Young's moduli of the fibre and the matrix, respectively, ν is the SiC Poisson's ratio ($\nu \approx \nu_f \approx \nu_m \approx 0.2$), and R_f is the fibre radius ($R_f \approx 7$ μm). $\delta\Delta$ was measured on the last cycle before the failure. N is the number of matrix cracks. It has been measured by optical microscopy on polished longitudinal sections of the failed minicomposites after chemical etching (Murakami reactant) in order to reveal the matrix microcracks closed during unloading.

The second method considers the matrix crack spacing distance l_s ($= N/L_g$). τ is given by Eq. (2).[9,10]

$$\tau = \frac{\sigma_s R_f}{2V_f l_s\left(1 + \frac{E_f V_f}{E_m V_m}\right)} \quad (2)$$

where σ_s is the applied stress at matrix cracking saturation and V_m the matrix volume fraction ($V_m \approx 1 - V_f$). In the present case, because of a low fibre volume fraction ($V_f \approx 0.2$), the minicomposites failed before reaching the cracking saturation. Therefore, σ_s was similar to the failure stress.

After ultimate failure, the morphology of the fracture surfaces was observed with a scanning electron microscope (SEM) (HITACHI S800).

2.4.2. Oxidation tests

In order to study the oxidation resistance of the interphases, the minicomposites were submitted to thermal ageing in air under a static loading following a procedure similar to that described by Lebrun et al.[11] Each specimen, with a 50 mm gauge length, was vertically maintained in the hot area of a furnace between two alumina tubes with an alumina-based adhesive (Aremco ref. 603, USA). At each alumina rod ends, hooks allowed device self-alignment. Once the temperature reached the set-point of 700°C, a 9.5 kg load (corresponding to a force of 93 N) was very carefully hooked to the bottom end of the alumina tube in the cold area. The specimen lifetime (i.e. the time before failure) was automatically measured by means of a switch connected with a timer which detects the load fall. The test originality lied in the possibility to expose the minicomposite either to a dry air stream (from the top to the bottom) obtained from liquid air evaporation or to a moist air obtained by sparging in 40°C liquid water. In the case of moist air, the air inlet pipe was maintained at 50°C between the sparger and the furnace; this device ensured constant moisture content for each experiment.

2.4.3. BN microstructure and texture

Thin longitudinal sections of minicomposites after tensile test were studied by transmission electron microscopy (TEM: Topcon 002B, Japan) using bright-field, high resolution (HR) and selected area diffraction (SAD) techniques. The samples were embedded in a ceramic cement and mechanically thinned. The thin sheets were then ion-milled (600 Duo Mill from Gatan, USA) until the electron transparency.

3. Results

3.1. Mechanical behaviour

3.1.1. Tensile tests

Average tensile mechanical characteristics at ambient temperature for the four batches of minicomposites are presented in Table 1. Fig. 3 displays a typical force–strain

Table 1
Average tensile mechanical characteristics of each batch of minicomposites.[a]

Batch	r (m/h)	ε_{PL} (%)	F_{PL} (N)	ε_F (%)	F_F (N)
0 (PyC)	6	0.09	111	0.56	169
1	2	0.04	59	0.35	128
2	2.5	0.10	119	0.53	167
3	3	0.06	83	0.55	137

[a] ε_{PL} and F_{PL} are the proportional limit and force, ε_F and F_F are the strain and force at failure

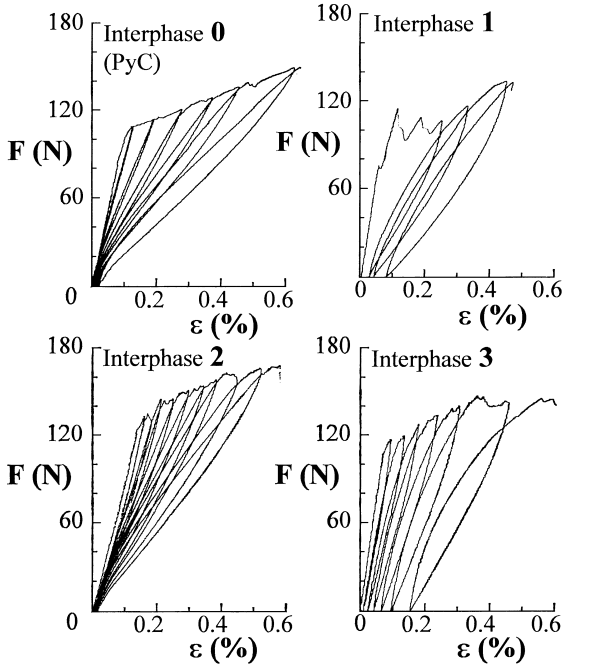

Fig. 3. Typical tensile force–strain curves with unloading-reloading cycles for minicomposites with different kinds of interphases.

curve for each kind of interphase. In every case, an extended non-linear domain evidencing matrix microcracking and fibre/matrix debonding follows the initial linear elastic region. Therefore, the four kinds of interphase act as mechanical fuses.

Minicomposites of batches 0 and 2 exhibit similar tensile behaviours with small residual stresses. The identical average failure forces for both batches are the highest. Therefore, BN interphase 2 processed with $r = 2.5$ m/h is as good at room temperature as reference PyC interphase. Batch 3 obtained with $r = 3$ m/h exhibits weakest mechanical properties with important residual strains evidencing that the fibre/matrix load transfer is less good. The characteristics decrease more for batch 1 interphase prepared with the slowest rate of tow travelling. Thus, with these processing conditions, the intermediate r of 2.5 m/h appears to result in an optimum.

The average proportional limit force for each batch evolves in the same way. These results need not mean that for the best composites (batches 0 and 2) the matrix begins to crack later during the composite tension. But, as the load transfer is better, the very first crack coming out does not lead to a deflection from linearity detectable on curves at low load level.

3.1.2. Interfacial shear stress τ

Interfacial shear stresses measured by following the different methods (Table 2) bear out the different interphase characteristics. However, a distinction appears between batches 0 and 2. If the fibre/matrix bond is strong with PyC interphase, the lowest τ values obtained with batch 2 show that the BN coating results in an intermediate bond.

3.1.3. SEM observation of fracture surfaces

SEM observation of batch 1 minicomposite fracture surfaces after tensile tests [Fig. 4(a)] shows an important fibre pull-out. The pull-out lengths can exceed 200 μm. The surface of the pulled out fibres is smooth and free of any coating. The debonding occurs in the fibre/interphase interface as evidenced by highest magnification observation [Fig. 4(b)]. This large debonding corroborates the measured low value of τ.

In the case of batch 2, the fibre pull-out is small and generally lower than 50 μm evidencing the strongest fibre/matrix bonding. Here, the interphase remains well fixed on the fibre as shown in Fig. 5(a) where the rough and tortured BN coating surface appears. A highest magnification observation [Fig. 5(b)] shows a debonding that occurs within the interphase itself.

Concerning batch 3 [Fig. 6(a)], the pull-out lengths are medium (reaching 100 μm). If the surface of the pulled out fibres seems to be smooth as in the case of batch 1, a meticulous observation shows that they are not bare but coated with the whole BN interphase [Fig. 6(b)]. Here, the debonding occurs near the matrix.

3.2. TEM characterization

3.2.1. Batch 2 minicomposite

Bright-field observation of interphase 2 (Fig. 7) shows that it is made of two sublayers with different textures

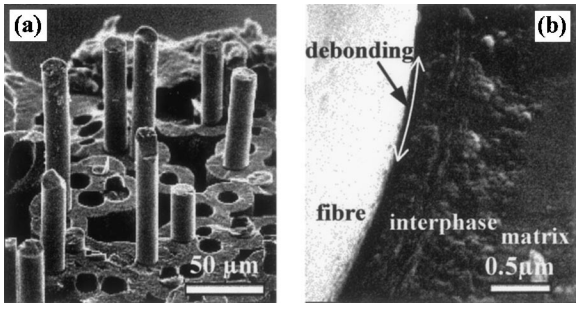

Fig. 4. SEM obsevations of the failure surface of a batch 1 minicomposite: (a) important fibre pull-out; (b) debonding in the fibre/interphase interface.

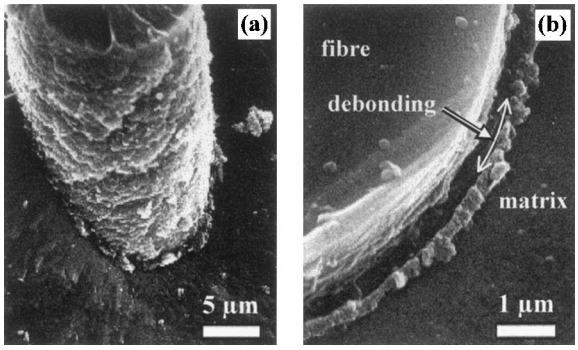

Fig. 5. SEM observations of the failure of a batch 2 minicomposite: (a) part of BN coating fixed on pull-out fibre; (b) debonding within the interphase.

Table 2
Average interfacial shear stresses τ

batch	V'_p(%)	l_s(μm)	N	E_0(GPa)	σ_s(MPa)	σ_p(MPa)	σ'(MPa)	$\delta\Delta$(μm)	τ (MPa)	
									Eq. (1)	Eq. (2)
0 (PyC)	22.9	87	462	350	503	455	223	31	117	73
1	18.4	408	98	348	306	311	155	41	15	12
2	19.2	206	194	305	417	409	200	24	75	32
3	17.5	279	143	328	269	255	128	32	29	20

and equivalent in thickness. The total interphase thickness is about 450 nm. While the interface between both sublayers is regular and linear, the interphase/matrix interface appears on this scale irregular (''serrated'') owing to the growth of extended coherent domains (corresponding to high bright/dark contrast areas) where BN organisation is very high. On the contrary, the weak contrast of the second sublayer located near the fibre evidences a poorer crystallographical organisation.

The SAD patterns performed in both sublayers (Fig. 8) are typical, with their 002 arcs, of an anisotropic turbostratic material. For the sublayer located near the matrix, spots occurrence in the SAD pattern reveals the local existence of BN submicrometric polycrystalline structures. Furthermore, the smaller arc length (or arc-opening angle in azimuth) evidences a better 002 planes average orientation than near the fibre.

HR observation of fibre/BN interface (Fig. 9, left) shows that it is made of a thin amorphous sublayer (thickness < 5 nm). This layer can (i) either result from a Hi-Nicalon fibre surface carbon enrichment,[12–14] or (ii) be BN that begins to depositate on the fibre in amorphous form. In any cases, this interface observation (performed after mechanical test) does not reveal any debonding.

Close to the fibre surface, the deposited BN appears first poorly organised with limited coherent domains and 002 planes orientated at random. Then, the degree of structural anisotropy increases progressively from the fibre to the interface of both interphase sublayers (i.e. Fig. 9, from the left to the right): the coherent domains expand along stacking *c* axis (ranging from 10 to 15 fringes) as well as longitudinally (parallel to the fibre axis) (fringes length ~10 nm) (Fig. 10, left). Thus, a structural gradient is evidenced within the first BN interphase sublayer.

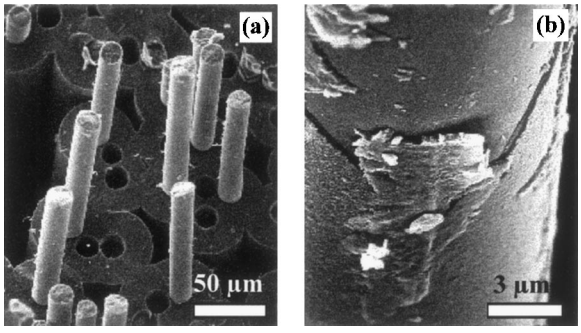

Fig. 6. SEM observations of the failure surface batch 3 minicomposite: (a) smooth pulled out fibres; (b) BN interphase fixed on pulled out fibre.

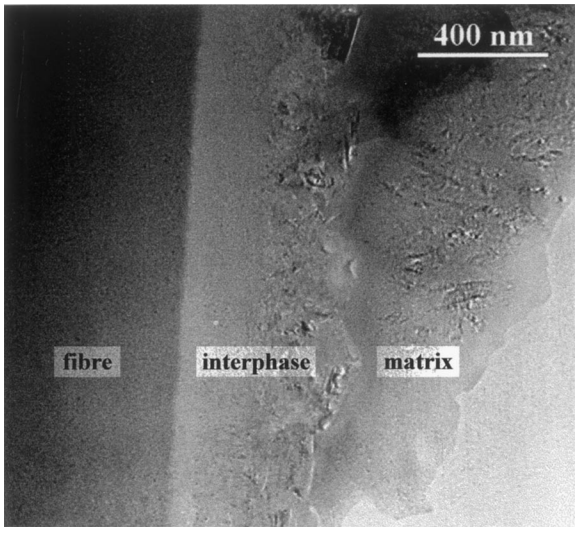

Fig. 7. Bright field TEM image of the interphase of a batch 2 minicomposite.

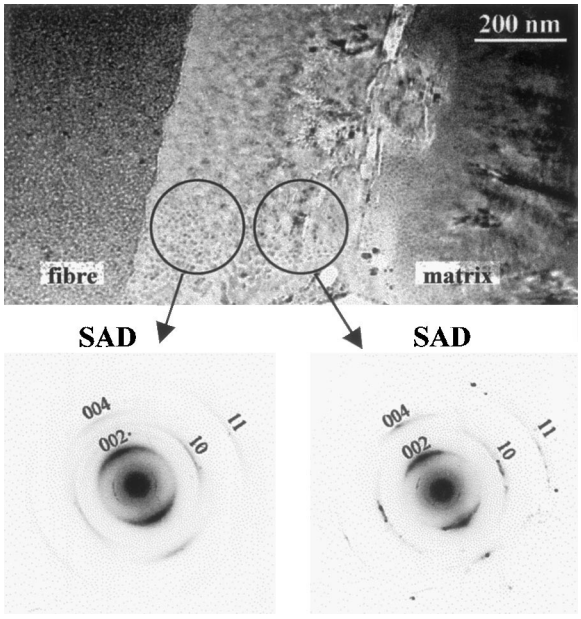

Fig. 8. Bright-field TEM image of the interfacial zone of a batch 2 minicomposite and corresponding SAD patterns (negatives).

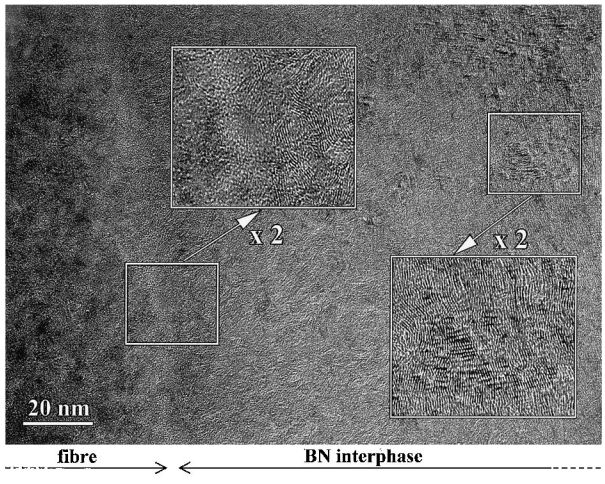

Fig. 9. HR-TEM image of the interphase of a batch 2 minicomposite near the fibre.

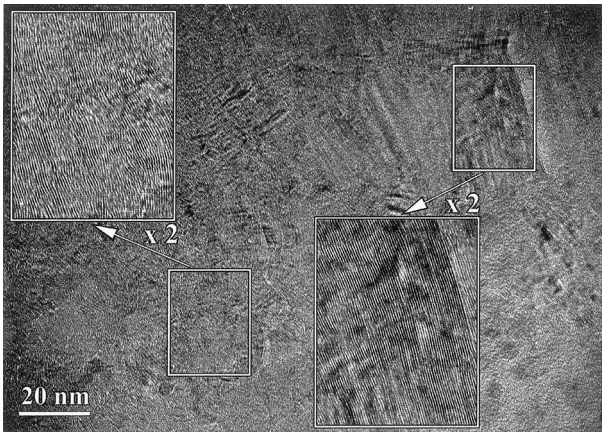

Fig. 10. HR-TEM image of the middle of the interphase of a batch 2 minicomposite.

The observation of the second sublayer located near the matrix (Fig. 10, right) reveals a very high structural organisation even if some 002 fringe distortions still remain. The fringes can exceed 50 nm in length. These large coherent domain sizes explain the sublayer thickness inhomogeneity and consequently the interphase/matrix interface irregularity.

3.2.2. Batch 1 minicomposite

As in the case of batch 2, batch 1 minicomposite study (Fig. 11) evidences the occurrence of two sublayers. As expected because of the slower rate of tow travelling ($r = 2$ m/h for batch 1 against 2.5 m/h for batch 2) and hence a higher reactor resident time, the total interphase thickness is higher: about 950 nm. But here, the second sublayer located near the matrix is homogeneous in thickness. Another important difference: in addition, two dark "edges" appear at the fibre/interphase interface with a large debonding located between the both; this debonding extends over long distances.

From a comparison between a SAD performed on these dark edges and a SAD performed more inside the fibre (Fig. 12, bottom), it is clear that the SiC fibre surface has been crystallised. Both SAD patterns are typical of SiC but, whereas diffraction rings are quasi-continuous within the fibre (SiC nanometric grains size), these are spotted at the fibre surface (more extended SiC grains size). This crystallisation has not been observed in batch 2. For batch 1, it can be due to a slower rate of tow displacement, which gives the fibre enough time to be raised to a highest temperature while going through the reactor hottest area (~1250°C). This thermal treatment is responsible for the fibre crystallisation that starts from its surface, causes local embrittlement and results in a large debonding.

SAD observations of interphase (Fig. 12, top) show that the first BN sublayer (located near the fibre) is identical with that of batch 2: it is an anisotropic turbostratic BN. On the contrary, the second sublayer

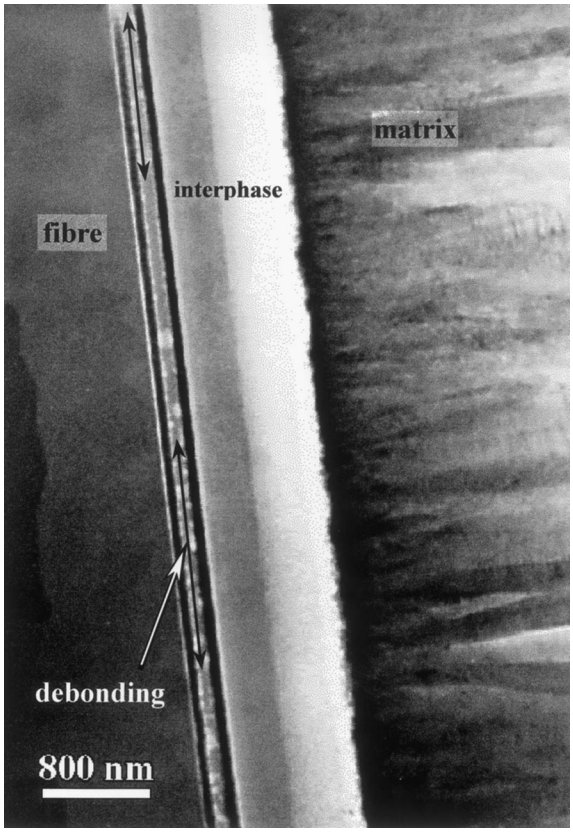

Fig. 11. Bright-field TEM image of the interphase of a batch 1 minicomposite.

(located near the matrix) is made of an isotropic BN, 002 diffraction arcs meet together and form continuous rings; there is no more preferential orientation. Here again, this difference with batch 2 can be explained by the slower rate of tow displacement. The gaseous phase infiltrated in the tow porosity is drag off more slowly to the hottest areas, which allows it to be raised to a highest temperature. Homogeneous nucleation can be then favoured to the detriment of heterogeneous chemical surface reactions. This phenomenon associated with a high yield of homogeneous reaction, results in an important production of HF and intermediate species and consequently leads to a material disorganisation.

3.2.3. Batch 3 minicomposite

Batch 3 interphase is also made of two sublayers (Fig. 13): a first preponderant one located near the fibre identical with those of the other batches, about 250 nm in thickness, and a very thin one located near the matrix (about 20 nm in thickness) where BN organisation is very pronounced. The faster tow rate (3 m/h) can explain this disproportion. The fibre resident time in the hottest area is reduced; the second organised sublayer has no more time to grow as in the case of batch 2. But, contrary to batch 2, this restricted growth allows this sublayer to keep a constant thickness and therefore to form a regular and linear interface with the matrix.

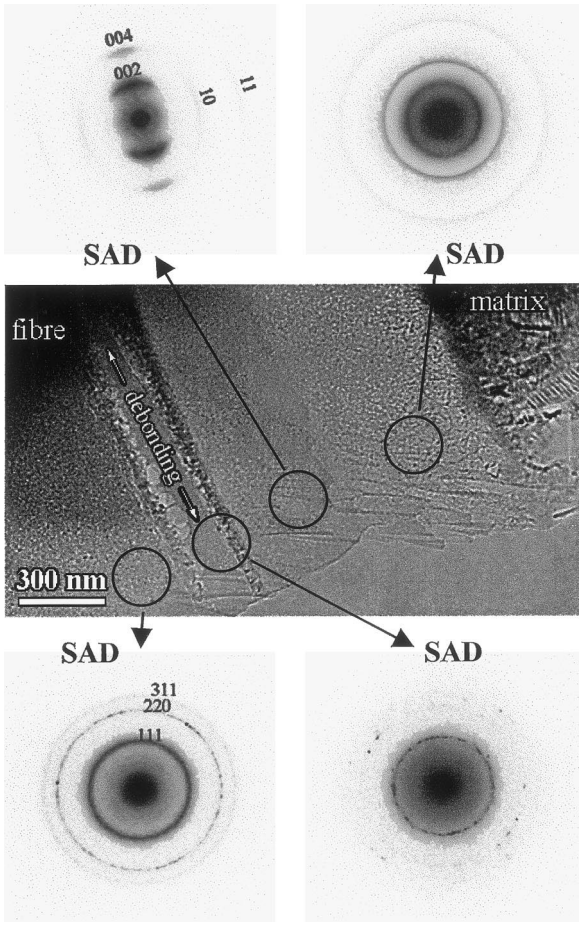

Fig. 12. Bright-field TEM image of the interfacial zone of a batch 1 minicomposite and corresponding SAD patterns (negatives).

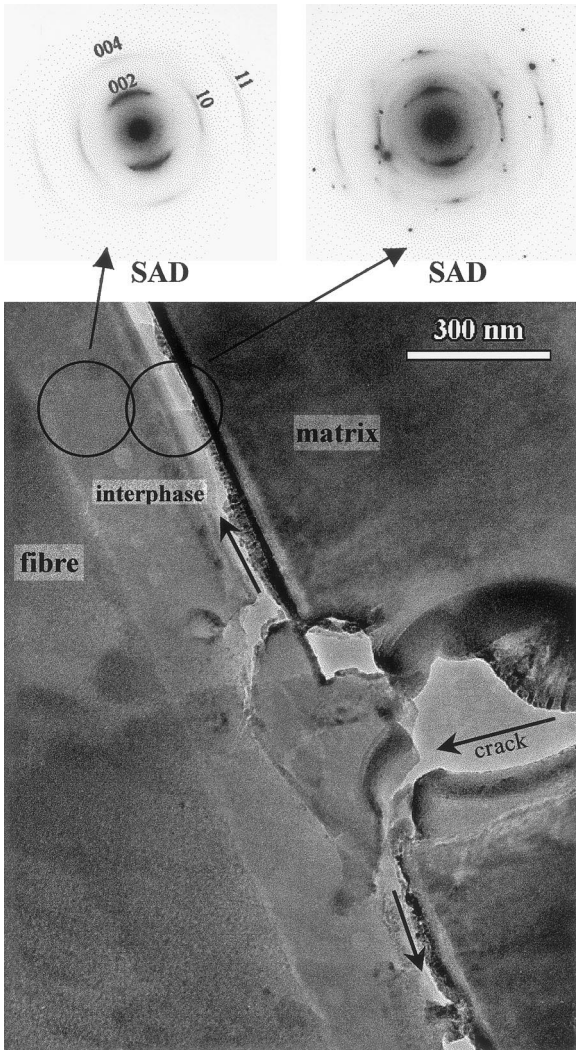

Fig. 13. Bright-field TEM image of the interfacial zone of a batch 2 minicomposite and corresponding SAD patterns (negatives).

Fig. 13 exhibits a deflection of a matrix crack: it occurs close to the matrix within this thin orientated sublayer. Because of interface regularity, the crack can propagates along the matrix in mode II over very long distances. This phenomenon explains SEM observations where the whole BN coating was found to remain fixed on the fibre with a smooth and regular surface.

3.3. Lifetime at high temperature under tensile loading

The average values of the lifetimes at 700°C in dry or moist air under a 9.5 kg load are reported in Table 3.

As a general rule, in these conditions, the minicomposite lifetimes depend on the ability of the interphase to protect the fibre from a mechanism of stress corrosion. Indeed, Bertrand et al.[15] have evidenced, thanks to similar tests performed on as-received bare fibre tows, that the Hi-Nicalon fibre lifetime becomes extremely short (below one minute for a tow submitted to a load of 4.5 kg!). Within a cracked matrix of a composite, if the interphase is oxidised the fibre is directly exposed to air and breaks, which results in the failure of the whole composite.

Table 3
Average lifetimes, at 700°C, under a 9.5 kg load, of the minicomposites

Batch	Lifetime (h)	
	Dry air	Moist air
0 (PyC)	3	5
1	47	7
2	89	62
3	>400	187

For all the minicomposites with BN interphases, the lifetimes are significantly improved which does prove the advantage of BN with respect to pyrocarbon both in dry air and moist air. Among the three batches, batch 3 allows to achieve the best results. In dry air the experiment had to be stop after 400 h of exposure, which evidences the very efficient protection.

4. Discussion

4.1. Relation between structures of fibre/matrix interfaces and minicomposite mechanical behaviour

From the above results, the processing parameter r appears to play a very important role in the structure of the resulting BN interphase and so in the control of the fibre/matrix bonding. Indeed, the resident time of the tow inside the hot areas and the gap between the actual fibre temperature and the susceptor temperature depends on r. Thus, with a high rate ($r > 2$ m/h), the fibre temperature does not have time to reach the susceptor temperature and does not follow exactly the temperature profile presented in Fig. 2.

Concerning batch 2, the BN coating located close to the matrix is made of very well organised BN domains. A slow enough rate of displacement tow ($r = 2.5$ m/h) allows the large extension of the domains. The result is a rough interphase surface and an irregular BN/matrix interface and consequently a good bonding of the matrix. During deflections of matrix cracks from mode I to mode II occurring in the course of unloading-reloading cycles, intense frictions (cf. τ values) between two rough surfaces restrict the sliding. These frictions and tearing result in a SEM observation of a tortured interphase surface fixed on pulled out fibres. These features explain that, among the three BN interphases, interphase 2 confers the best mechanical properties.

When r increases up to 3 m/h (batch 3), the well-organised sublayer does not have time to thicken; it remains thin and regular. Hence, debonding and sliding can occur over long distances without any obstacles. As a matter of fact, the surface coating of the pulled out fibres appears smooth on SEM examinations. The interfacial shear stress is weak and so are the mechanical properties.

Previous studies on CMCs with a PyC interphase[16,17] have already reported the importance of tailoring the interphase thickness and orientation. But, whereas a thick well-organised pyrocarbon results in a too weak fibre/matrix bonding, here a sufficient highly crystallised BN thickness allows, on the contrary, to limit the sliding.

For slowest rates of displacement tow ($r = 2$ m/h) (batch 1), the second BN sublayer located near the matrix becomes isotropic because of a more important homogeneous nucleation; but above all, the fibre surface starts to crystallise by thermal treatment. This feature is surprising for the Hi-Nicalon fibre is expected to be thermodynamically stable owing to its poor content of oxygen.[18–20] Nevertheless, a recent study[12] performed on heat-treated Hi-Nicalon fibres has shown that a growth of the β-SiC crystallite size occurs in the bulk from and above 1300°C resulting in a mechanical enhancement of the fibre. In the present case, the particular treatment (rather short time at a temperature close to the pivot point of 1300°C) limits the crystallisation to the fibre surface. This local inhomogeneity involves a local embrittlement instead of global reinforcement and so an important fibre pull-out. The fibre/matrix bonding becomes very weak (low τ values) and the load transfer from the matrix to the fibre is no more ensured.

A schematic representation, which summarises the different structures and the fracture behaviour of the BN interphases, is given in Fig. 14.

4.2. Lifetime

As expected, the lifetime of the reference batch 0 with a pyrocarbon interphase is not very dependent on the moisture content and is the shortest despite an applied

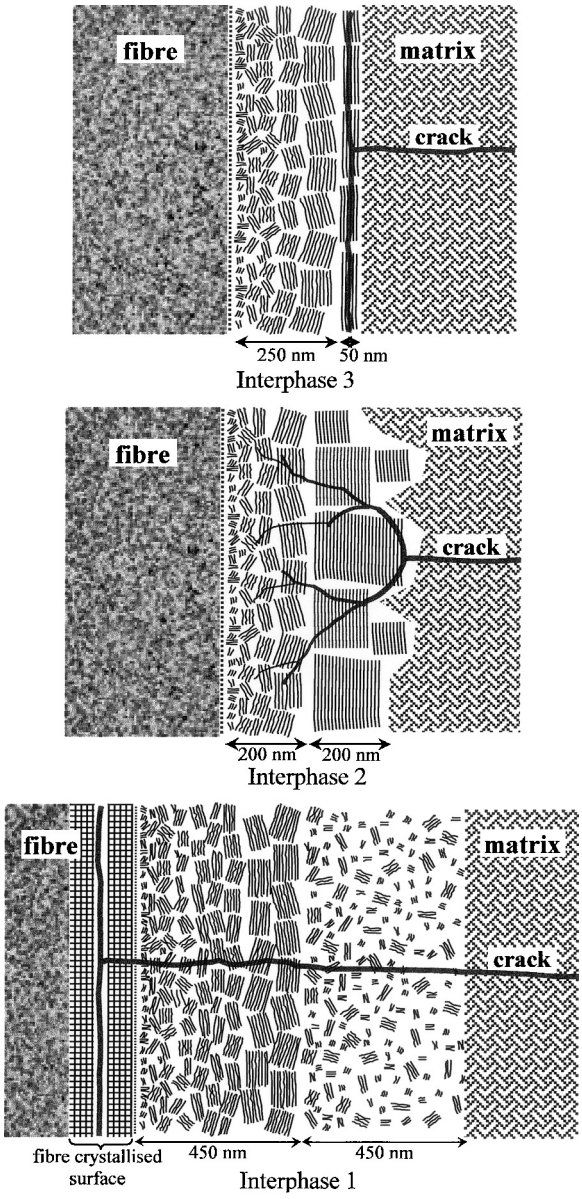

Fig. 14. Schematic representation of the BN interphases structures and the matrix cracks deflection.

force (93 N) below the apparent proportional limit (111 N). In these conditions, the composite failure results from a rapid oxidation of the PyC interphase by air oxygen into $CO(g)$ and/or $CO_2(g)$.[21]

Concerning the other batches, the protection of the BN interphase and consequently of the minicomposite fibres toward oxidation is due to the formation of a B_2O_3 layer. This glass acts as a physical barrier against oxygen. But, this protection depends on the moisture content. Indeed, water reacts with B_2O_3 to give volatile boric acids $HBO_2(g)$, $H_3BO_3(g)$, and $H_3B_3O_6(g)$, which decreases the protecting effect of the oxide layer.[22]

For batch 3, the matrix cracks are deflected close to the interphase/matrix interface i.e. "far" from the fibre at about 250 nm (Fig. 14, top). Although this behaviour is not favourable to the mechanical properties; it allows, in return, the fibre to be protected from air. For batch 2, the interphase/matrix bonding involves important tearing. Finally, cracks allows air to come nearer to the fibre (middle of Fig. 14) than in the case of batch 3, which decreases the lifetime. As for batch 1, the weak link is located in the fibre surface (Fig. 14, bottom); the fibre is of course quickly exposed; which results in an even shorter lifetime.

At this point, it is not possible to determine the best BN interphase. Indeed, even if the oxidation resistance is considerably improved compared with the reference, the best minicomposites at room temperature (batch 2) do not result in the best lifetimes at high temperature (those of batch 3). Hot dynamic cycle fatigue tests would allow to settle because the mechanical behaviour would play an even more important part than in static tests.

5. Conclusion

BN interphases with a structural gradient were prepared by using a one-step continuous dynamic CVI process within 1-D SiC/SiC minicomposites. The fibre tow travelled through a reactor that contains different hot areas (TG-CVI process). The infiltration occurred while keeping the same conditions of gaseous phase (pressure, flow rates, composition) during the whole experiment. A judicious choice of travelling rate combined with a well adapted temperature profile in the susceptor allowed to obtain minicomposites with good properties.

Indeed, tensile tests at room temperature have shown that the BN interphases act as mechanical fuses and that the fibres are not chemically degraded. These good results are obtained thanks to a fibre coating starting in a "low" temperature area. This non-aggressive treatment conditions protect the fibre. Then, while going through a hottest area, the structural anisotropy of the BN infiltrated in the tow can increase without fibre chemical attack. This organised BN allows the interphase to deflect the matrix cracks. The key role of the tow travelling rate has been confirmed. Indeed, the variation of the substrate temperature and the infiltrated gaseous phase depends upon this rate. As evidenced by TEM, the thickness, the textures, the homogeneity and the morphology of the different sublayers that constitute the whole final interphase hence depend on it, and, as a mater of fact, the global composite properties. Furthermore, a too slow passing through raises the fibre to a too high temperature, the fibre surface undergoes a local crystallisation which results in an intense debonding.

Finally, thermal ageing tests in dry or moist air under a static loading have confirmed that the BN interphases significantly improve the lifetimes of the minicomposites compared with a classical pyrocarbon interphase.

References

1. Evans, A. G. and Zok, F. W., The physics and mechanics of fibre-reinforced brittle matrix composites. *J. Mater. Sci.*, 1994, **29**, 3857–3896.
2. Rebillat, F., Guette, A., Espitalier, L., Debieuvre, C. and Naslain, R., Oxidation resistance of SiC/SiC minicomposites with a highly crystallised BN interphase. *J. Eur. Ceram Soc.*, 1998, **18**, 1809–1819.
3. Rebillat, F., Guette, A. and Brosse, C. R., Chemical and mechanical alterations of SiC Nicalon fiber properties during the CVD/CVI process for boron nitride. *Acta Mater.*, 1999, **47**(5), 1685–1696.
4. Vincent, H., Lopez-Marure, A., Lamouroux, F., Vincent, C., and Bouix, J., Continuous elaboration of boron nitride on SiC (Hi-Nicalon) fiber. Textures of deposited BN and properties of coated fibers. In *Proceedings of the 11th Journées Nationales sur les composites*, J. Lamon, and D. Baptiste, D. 18–20 November, Arcachon, France, 1998, pp. 393–404.
5. Lopez-Marure, A., *La Réalisation et le Comportement d'Interphases BN à Gradient de Propriétés, Application à des Composites Céramiques.* PhD thesis, University of Claude Bernard Lyon 1, France, 1999.
6. Olivier, C., Elaboration et Etude du Comportement Mécanique de Composites Unidirectionnels C/Si_3N_4 et SiC/Si_3N_4. PhD thesis, Institut National des Sciences Appliquées of Lyon, France, 1998.
7. Bertrand, S., Forio, P., Pailler, R. and Lamon, J., Hi-Nicalon/SiC minicomposites with $(Pyrocarbon/SiC)_n$ Nanoscale multilayered interphases. *J. Am. Ceram. Soc.*, 1999, **82**(9), 2465–2476.
8. Lamon, J., Rebillat, F. and Evans, A. G., Microcomposite test procedure for evaluating the interface properties of ceramic matrix composites. *J. Am. Ceram. Soc.*, 1995, **78**(2), 401–405.
9. Marshall, D. B. and Evans, A. G., Failure Mechanisms in Ceramic-Fiber/Ceramic-Matrix Composites. *J. Am. Ceram. Soc.*, 1985, **68**(5), 225–231.
10. Aveston, J., Cooper, G.A. and Kelly, A., Single and multiple fracture. In *Proceedings of the Conference of the National Physical Laboratory, the Properties of Fiber Composites*, IPC Science and Technology Press Ltd, Surrey, UK, 1971, pp. 15–26.
11. Lebrun, G.A. and Lamon, J., Influence de la distribution spatiale des fibres au sein d'un composite sur le comportement mécanique en traction. In *Annales des Composites*, 1995/4. AMAC, 1995, pp. 121–130.
12. Bertrand, S., Lamon, J., Pailler, R. and Goujard, S., Effect of heat-treatments on the microstructure and the properties of Hi-Nicalon fibres. *J. Eur. Ceram. Soc.*, submitted for publication.

13. Bansal, N. P., Effects of HF treatments on tensile strength of Hi-Nicalon fibres. *J. Mater. Sci.*, 1998, **33**(17), 4287–4295.
14. Bansal, N. P. and Chen, Y. L., Chemical, mechanical and microstructural characterization of low-oxygen containing silicon carbide fibers with ceramic coatings. *J. Mater. Sci.*, 1998, **33**(22), 5277–5289.
15. Bertrand, S., Lamon, J. and Pailler, R., Oxidation resistance in static fatigue conditions of Hi-Nicalon fibre tows and SiC/(PyC–SiC)$_n$/SiC minicomposites. *J. Eur. Ceram. Soc.*, submitted for publication.
16. Nguyen Van Sang-Trouvat, B., *Analyse et Optimisation des Interfaces dans les Composites Carbone/Carbone à Renfort Fibreux*. PhD thesis no. 1635, University of Bordeaux I, France, 1996.
17. Olivier, C., Veyret, J. B. and Vidal Setif, M. H., Mechanical properties of Hi-Nicalon fibre-reinforced silicon nitride composites. *Key Engineering Materials*, 1997, **127–131**(2), 753–760.
18. Takeda, M., Imai, Y., Ichikawa, H., Ichikawa, T., Kasai, N., Seguchi T. and Okamura, K., Thermomechanical analysis of the low oxygen silicon carbide fibers derived from polycarbosilane. In *Proceedings of the 17th Annual Conference on Composites and Advanced Ceramic Materials*, in *Ceram. Eng. & Sci. Proc.*, ed. D.C. Cranner. 10–15 January, Cocoa Beach. American Ceramic Society, 1993, pp. 540-547.
19. Shimoo, T., Tsukada, I., Narisawa, M., Seguchi, T. and Okamura, K., Change in properties of polycarbosilane-derived SiC fibers at high temperatures. *J. Ceram. Soc. of Japan*, 1997, **105**(7), 559–563.
20. Chollon, G., Pailler, R., Naslain, R., Laanani, F., Monthioux, M. and Olry, P., Thermal stability of a PCS-derived SiC fiber with a low oxygen content (Hi-Nicalon). *J. Mater. Sci.*, 1997, **32**, 327–347.
21. Fillipuzi, L., Camus, G., Naslain, R. and Thebault, J., Oxidation mechanisms and kinetics of 1D-SiC/C/SiC composite materials: 1 — an experimental approach. *J. Am. Ceram. Soc.*, 1994, **77**(2), 459–466.
22. Jacobson, N. S., Morscher, G. N., Bryant, D. R. and Tressler, R. E., High-temperature oxidation of boron nitride: II, boron nitride layers in composites. *J. Am. Ceram. Soc.*, 1999, **82**(6), 1473–1482.